



Microstructure, mechanical properties and stretch formability of as-rolled Mg alloys with Zn and Er additions

Ke Liu* , Jing-Tao Liang, Wen-Bo Du, Shu-Bo Li, Zhao-Hui Wang, Zi-Jian Yu, Jin-Xue Liu

Received: 12 November 2018/Revised: 12 April 2019/Accepted: 25 April 2020/Published online: 23 June 2020
© The Nonferrous Metals Society of China and Springer-Verlag GmbH Germany, part of Springer Nature 2020

Abstract The magnesium alloy has a unique advantage in 3C fields due to its high specific strength and excellent electromagnetic shielding characteristic. However, it is difficult to deform homogeneously because of hexagonal close-packed structure. In the present work, the microstructure, mechanical properties and stretch formability of magnesium alloy sheets with different alloying elements were investigated. It was indicated that a trace addition of Zn or/and Er made a key role in modifying texture, activating shear bands formation and precipitating nanoscale second phases, respectively, which resulted in an obvious improvement in both stretch formability and mechanical properties. The results suggested that the Mg–0.5Zn–0.5Er alloy sheet exhibited higher tensile strength along the rolling direction, i.e., yield strength of 180 MPa and ultimate tensile strength of 201 MPa, accompanying with superior Erichsen value of 7.0 mm at room temperature. The good performances of the sheet were ascribed to weakening basal texture intensity, formation of shear bands and precipitation of nanoscale W-phase ($Mg_3Zn_3Er_2$).

Keywords Mg–Zn–Er alloy; Hot rolling; Texture; Shear band; Stretch formability

1 Introduction

As a lightweight structural material, the wrought magnesium alloy has a unique advantage in 3C fields due to its high specific strength and excellent electromagnetic shielding characteristic [1]. However, as the hexagonal close packed (hcp) structure, it is difficult to make the magnesium alloy undergo a homogeneous deformation. In general, the wrought magnesium alloy has a strong basal texture and a notable anisotropy, which is harmful to the formability [2–4]. Modifying texture is one of key factors to improve formability at room temperature. Hot plastic deformation is an important way to weaken the basal texture via dynamic recrystallization (DRX), especially for an equal channel angular pressing (ECAP) [5, 6] and a differential speed rolling (DSR) [7, 8]. The as-wrought magnesium alloy therefore exhibits high performance such as high-strength, high-plasticity and high-formability capabilities. The high performances are ascribed to the grain refinement, texture modification and nanoscale precipitates. Besides, a great number of shear deformation bands and an abroad angular distribution of basal planes are introduced during deformation, which also advances mechanical properties as well as formability of magnesium alloys obviously.

Also, some alloying elements additions have an effective influence on the modification of texture. The rare earth element (RE) is one of the most important elements for the texture modification with its addition less than 1 wt% [9–13]. As reported, the addition of RE could decrease the values of both c/a and critical resolved shear stress (CRSS) of non-basal slip, respectively [9]. Additionally, the RE addition activates the number of shear bands by the deformation twin formation, especially for a $\{10\bar{1}1\}$ –

K. Liu*, J.-T. Liang, W.-B. Du, S.-B. Li, Z.-H. Wang, Z.-J. Yu
College of Materials Science and Engineering, Beijing
University of Technology, Beijing 100124, China
e-mail: lk@bjut.edu.cn

J.-X. Liu
Zhengzhou Light Metal Research Institute, Zhengzhou 450041,
China

{10 $\bar{1}2$ } double twin, which contributes to a random texture [11]. It reported that the addition of RE elements led to weak sheet textures, and consequently the ductility increased by reducing the anisotropy for conventional magnesium alloy sheets [14]. It is considered that the hard deformation mechanisms of non-basal slips are promoted when the basal slip and tensile twinning become exhausted. Besides, the addition of RE elements extremely restricts the DRX because of the segregation of RE in grain boundaries, which is responsible for the random texture partly [13, 15].

The Mg–Zn–Er alloys have been investigated in our previous studies. It is found that some primary second phases including I-phase (Mg₃Zn₆Er) and W-phase (Mg₃Zn₃Er₂) are generally coarse and distribute non-homogeneously, which are harmful to mechanical properties, while it is difficult to escape from their formation [16, 17]. Hot extrusion can destroy the coarse second phase effectively, and the as-extruded Mg–Zn–Er alloys containing I-phase/W-phase display relatively high mechanical properties [18–20]. Although the as-extruded Mg–Zn–Er alloys exhibit good performance in mechanical properties, it is still found that the coarse second phases are the main fracture cores [20]. The presence of the coarse second phase is injurious for the stretch formability in the same manner. Therefore, in this work, three kinds of magnesium alloys, i.e., Mg–0.5Zn, Mg–0.5Zn–0.5Er and Mg–3Zn–0.5Er (wt%), were designed and then solution-treated in order to investigate the elements effect on the microstructure, mechanical properties and stretch formability of magnesium alloys without coarse second phases. The results suggested that the trace addition simultaneously of Zn and Er would lead to the modification of texture, formation of shear bands and precipitation of nanoscale W-phase. Consequently, the stretch formability and mechanical properties of this alloy are advanced at room temperature.

2 Experimental

The as-cast alloys were prepared from pure Mg (99.99 wt%), pure Zn (99.9 wt%) and Mg-30 wt% Er master alloys with a graphite crucible in an electric resistance furnace under an anti-oxidizing flux. About 1200 g melting was poured into a steel mold. The ingot was 220 mm × 140 mm × 35 mm in size. In order to eliminate the coarse second phase, the as-cast samples were annealed at 460 °C for 10 h and cooled down in 70 °C water. Then, the ingots were subsequently machined into slabs with dimensions of 100 mm × 60 mm × 8 mm. The

Table 1 Chemical compositions of magnesium alloys

Nominal compositions	Chemical compositions/wt%			Zn/Er
	Zn	Er	Mg	
Mg-0.5Zn	0.51	0	Bal.	–
Mg–0.5Zn–0.5Er	0.62	0.56	Bal.	1.11
Mg–3Zn–0.5Er	3.06	0.46	Bal.	6.65

slabs were hot-rolled into sheets from 8.0 to 2.8 mm with a rolling speed of 32 mm·s^{−1} under a reduction of 10%–15% per pass at 400 °C. The cumulative rolling reduction was ~ 65%.

The chemical compositions of magnesium alloys were analyzed by using an X-ray fluorescence (XRF, Magix-PW2403) analyzer, and the nominal compositions as well as actual chemical composition are shown in Table 1. The microstructural observation was carried out by using an optical microscope (OM, Zeiss-Imager.A2m) and a transmission electron microscope (TEM, JEM-2000FX, JEOL), respectively. A selected area electron diffraction (SAED) pattern and an energy-dispersive spectroscopy (EDS) were carried out during TEM observation, respectively. The samples for OM observation were mechanically polished and etched in a solution of 4 ml nitric acid and 96 ml ethanol. Specimens for TEM observation were prepared by using electro-polishing and ion beam milling at an angle of incidence less than 10°. The macroscopic texture of the (0002) plane pole figure was observed by using X-ray via Schulz reflection method. Moreover, the microscopic texture analyses (EBSD) were conducted by using a scanning electron microscope (TFE-SEM, JEOL JSM-6500F) operating at 30 kV equipped with a TSL-OIM Analysis 5 software. Samples for texture analysis were prepared by using electro-polishing with a solution of 60% methanol, 30% glycerol and 10% nitric acid at 25 °C (voltage of 3–11 V) for 10–30 s.

Tensile test was carried out by using a DNS-20 universal testing machine under a constant speed of 1.0 mm·min^{−1} at room temperature. Specimens for tensile test were manufactured with a size of 5 mm gauge in width and 25 mm in gauge length from the sheets in three orientations, i.e., rolling direction (RD), 45° to RD direction and transverse direction (TD), respectively. Three parallel specimens were tested for each sample. The stretch formability of sheets with a square of ~ 60 mm was studied by using Erichsen tester, and the Erichsen value (IE) was a measurement of the punch stroke at fracture initiation. The Erichsen test used a hemispherical punch with a diameter of 20 mm at room temperature. The punch speed and blank-holder force were 35 mm·min^{−1} and 10 kN, respectively.

3 Results and discussion

3.1 Microstructure and macro-texture

Figure 1a–c shows OM images of as-rolled Mg–0.5Zn, Mg–0.5Zn–0.5Er and Mg–3Zn–0.5Er alloys. Figure 1a suggests that Mg–0.5Zn alloy is composed of recrystallized grains completely. Some recrystallized grains also contain lots of twins. Meanwhile, when a trace addition of Er is added, the microstructure of Mg–0.5Zn–0.5Er alloy is changed. It mainly consists of original grains which are elongated and crushed along the rolling direction after hot rolling (HR) process. Besides, there are lots of tiny grains being full of streamlined deformation bands in the Mg–0.5Zn–0.5Er alloy. The dilute addition of Er greatly can retard the growth of recrystallization grains by reducing the grain boundary mobility [9]. Furthermore, as the content of Zn increases to 3 wt%, the fully and finer recrystallized grains are present in the Mg–3Zn–0.5Er alloy compared with both Mg–0.5Zn alloy and Mg–0.5Zn–0.5Er alloy. It is suggested that the addition of Zn will lead to a positive misfit of grain boundaries, which would bring in a homogeneous recrystallization microstructure of magnesium alloys containing high content of Zn [21].

Figure 1d–f displays (0002) pole figures obtained from RD–ND plane of the as-rolled alloys. The macro-texture intensity of the alloys is 12.84 for Mg–0.5Zn, 6.51 for Mg–0.5Zn–0.5Er and 6.15 for Mg–3Zn–0.5Er alloys, respectively. The Mg–0.5Zn alloy has the strongest basal texture without spread of the (0002) orientation in the RD–TD plane, which is nearly twice as high as that of other Mg–Zn–Er alloys. The Mg–0.5Zn–0.5Er alloy exhibits a typical RD-split texture with double-peak intensity by about $\pm 15^\circ$

tilt of the basal pole in RD. The “split” texture might be caused by the mutual separation of the deformation bands and non-deformation band regions [22]. Moreover, the performance of texture of the Mg–3Zn–0.5Er alloy is very similar to that of the Mg–0.5Zn–0.5Er alloy. In conclusion, it is indicated that a trace addition of 0.5 wt% Er can play an effective role in modifying the basal texture of Mg–Zn system alloys, while the addition of Zn activates the occurrence of DRX completely.

3.2 EBSD analysis and precipitations

In order to study the microstructure in detail, EBSD measurement on as-rolled alloys was performed with a step size of 0.5. Figure 2a–c shows imaging quality (IQ) figures of the as-rolled alloys. The IQ indexing is used as a background. The boundaries of different twin types are highlighted by using different colors. The non-indexed areas correlating with high density of shear bands are present in black color. It stands for the grains suffering from high local strains. Therefore, the original indexing fraction for the raw EBSD data is $\sim 43\%$. The shear bands are composed of recrystallized grains and twins so that the high store energy as well as large orientation gradients is full of the substructure [23]. The shear bands appear like streamlines traversing across the image in the Mg–0.5Zn–0.5Er alloy obviously, as shown in Fig. 2b. As a result, a double-peak basal texture comes into being because of the intense shear strain localization [24]. Also, three kinds of twins are shown in IQ map marked with different colors, i.e., $\{10\bar{1}2\}$ extension twin boundaries at 86.3° (red color), $\{10\bar{1}1\}$ compression twin boundaries at 56° (blue color)

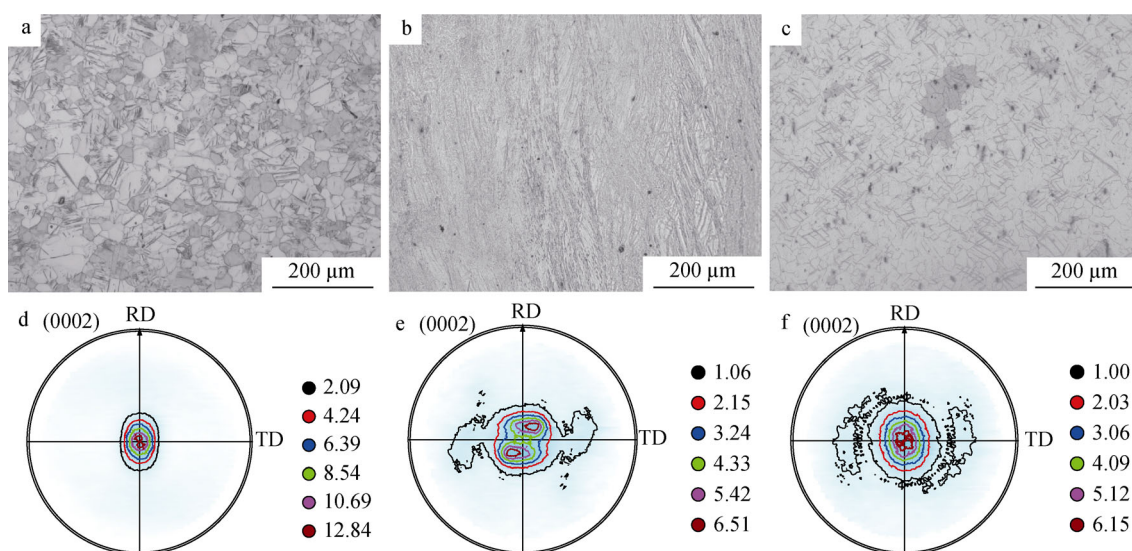


Fig. 1 OM images and macrotextures observed by XRD of **a, d** as-rolled Mg–0.5Zn alloy, **b, e** as-rolled Mg–0.5Zn–0.5Er alloy and **c, f** as-rolled Mg–3Zn–0.5Er alloy

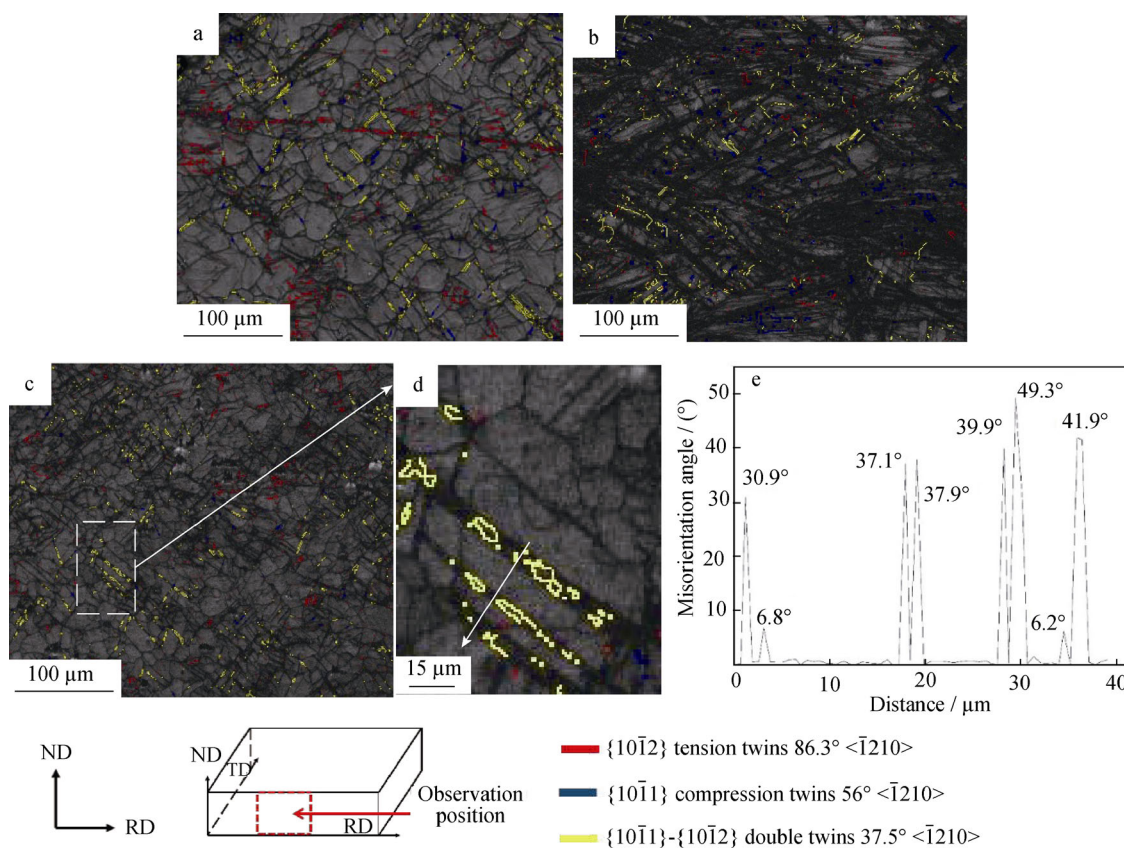


Fig. 2 IQ image of as-rolled **a** Mg-0.5Zn alloy, **b** Mg-0.5Zn-0.5Er alloy and **c** Mg-3Zn-0.5Er alloy; **d** IQ image at a high magnification corresponding to red rectangular in **c**, **e** misorientation along white arrow in **d** within grain

and {10 $\bar{1}$ 1}-{10 $\bar{1}$ 2} double twin boundaries at 37.5° (yellow color), respectively. The Mg-0.5Zn alloy contains a higher activity of extension twinning than Mg-0.5Zn-0.5Er and Mg-3Zn-0.5Er alloys. However, the numbers of compression twins locating near the shear bands are higher in Mg-0.5Zn-0.5Er alloy than in other two alloys. In addition, all the alloys include the dispersed double twins.

Figure 2d, e shows line profile of the misorientation angle across the grains along a white arrow (marked in Fig. 2d) direction in order to measure the crystallographic orientation relationships. The grains in the Mg-3Zn-0.5Er alloy are corresponding to the red rectangle in Fig. 2c. It is indicated that the measured misorientation angle slightly deviates from the theoretical value $\sim \pm 5^\circ$ due to the plastic rotation caused by dislocation slips [25]. There are some double twin boundaries (37.1°, 37.9°, 39.9° and 41.9°), random boundaries (30.9°, and 49.3°) and low angle grain boundaries (LAGBs, 6.8° and 6.2°) in the interior of grains. Apparently, the LAGBs and random boundaries are inside and near the double twins, respectively. The {10 $\bar{1}$ 1}-{10 $\bar{1}$ 2} double twin is easy to capture the basal and non-basal slip dislocations [26]. The strong slip activity of double twinning regions leads to a formation of the fine recovering substructure, forming a precursor stage

of the twin dynamic recrystallization (TDRX) [11, 27]. The twinned bands in the grains are considered to be micro-shear bands.

Figure 3 displays inverse pole figure (IPF) from EBSD measurements and corresponding (0001) pole figures (PF). Figure 3a-c suggests that Mg-0.5Zn and Mg-3Zn-0.5Er alloys are full of recrystallization microstructures, while Mg-0.5Zn-0.5Er alloy is permeated with serious distortion areas. The average grain sizes of Mg-0.5Zn and Mg-3Zn-0.5Er alloys are $\sim (53 \pm 0.9) \mu\text{m}$ and $(32 \pm 0.6) \mu\text{m}$, respectively. The values of the micro-texture intensity for Mg-0.5Zn, Mg-0.5Zn-0.5Er and Mg-3Zn-0.5Er alloys are 22.24, 15.41 and 12.26, respectively, as shown in Fig. 3d-f. The variation tendency of the microscopic texture agrees well with the macroscopic texture. It confirms that the addition of Er can weaken the basal texture and randomize the grain orientations [28]. It should be noted that the TDRX promotes the formation of shear bands via consuming the regions of compression/double twins in alloys containing Er [29]. So, the orientation of DRXed grains forming on both twins and shear bands is mostly random, but the non-DRXed grains left display a basal orientation after the last pass. As a result, the “tilted” basal texture is present in the Mg-0.5Zn-0.5Er and Mg-3Zn-

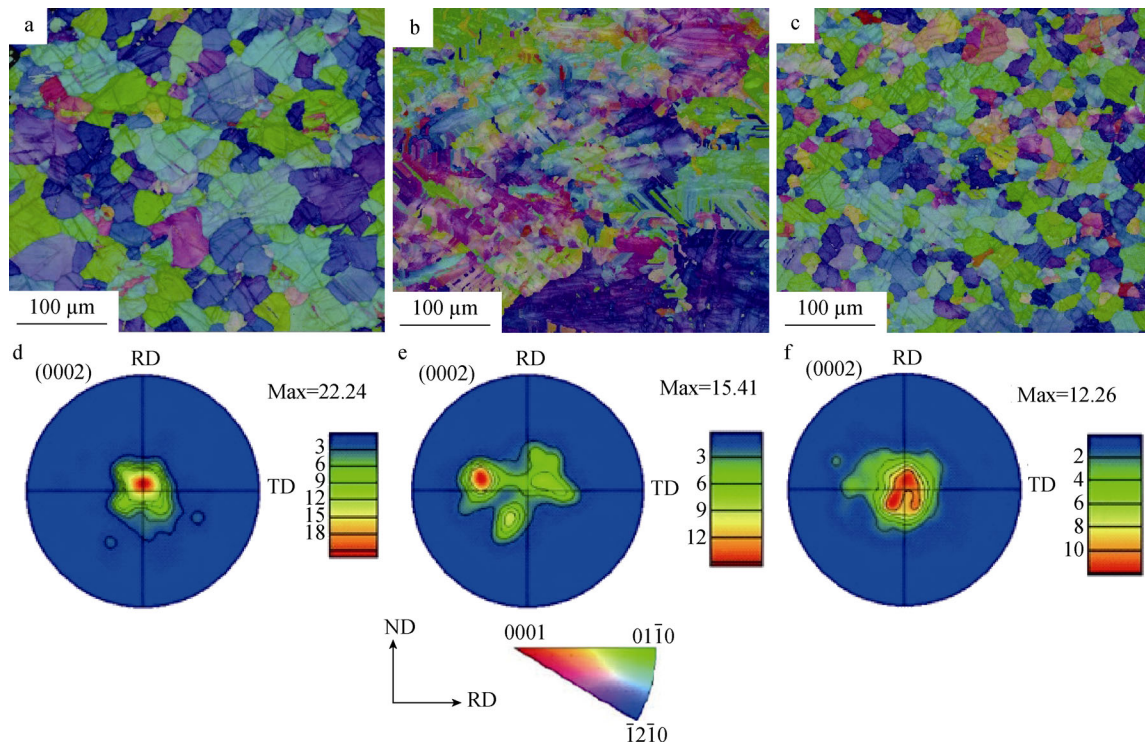


Fig. 3 IPF and PF observed by EBSD of **a, d** as-rolled Mg-0.5Zn alloy, **b, e** as-rolled Mg-0.5Zn-0.5Er alloy and **c, f** as-rolled Mg-3Zn-0.5Er alloy

0.5Er alloys, respectively. However, the increase in Zn content reduces the number of shear bands, which brings about a return of the texture peak point to the basal pole in the Mg-3Zn-0.5Er alloy.

Figure 4 shows TEM images of Mg-0.5Zn-0.5Er and Mg-3Zn-0.5Er alloy. Figure 4a shows plenty of fine DRXed grains (or sub-grains) and short rod-shaped dynamic nanoscale precipitates in the Mg-0.5Zn-0.5Er alloy. The nanoscale precipitates are the W-phase

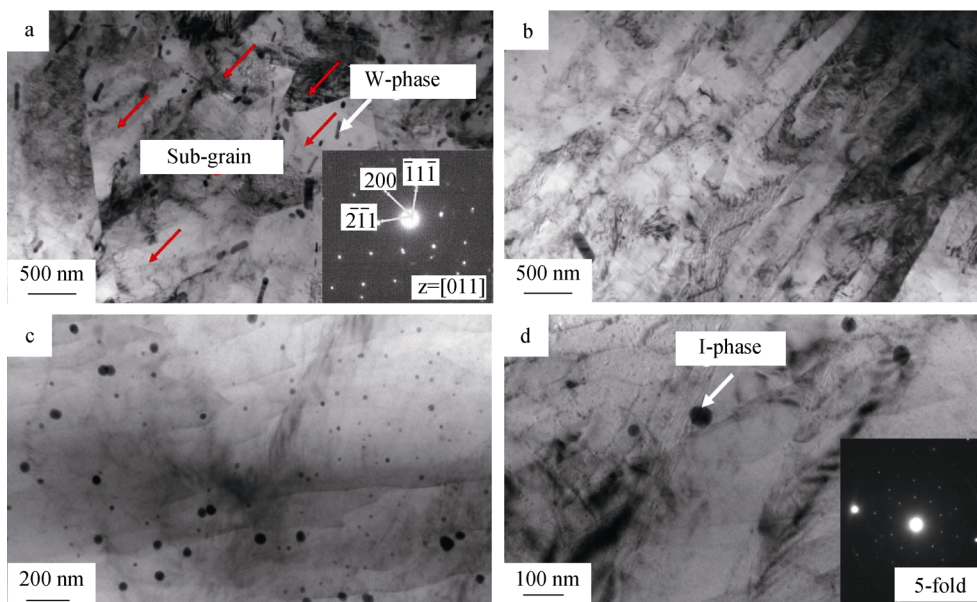


Fig. 4 TEM images of as-rolled Mg-Zn-Er alloys: **a** precipitates of nanoscale W-phase and its corresponding SAED patterns of Mg-0.5Zn-0.5Er alloy; **b** shear bands in Mg-0.5Zn-0.5Er alloy; **c** nanoscale I-phase in Mg-3Zn-0.5Er alloy; **d** I-phase and its corresponding SAED patterns with fivefold in Mg-3Zn-0.5Er alloy

Table 2 EDS analysis results of particles in Fig. 4 (at%)

Alloys	Mg	Zn	Er	Zn/Er
Mg–0.5Zn–0.5Er	76.20	15.30	8.49	1.80
Mg–3Zn–0.5Er	86.61	11.58	1.81	6.40

according to SAED pattern and EDS analysis (Zn/Er = 1.8 at%, as shown in Table 2) results. The W-phase with fcc structure results from a stronger segregation of solute elements in strain concentration regions during thermo-mechanical processing, which mainly distributes in sub-grain and grain boundaries rather than initial grain interiors (Fig. 4b) [21, 30]. The nanoscale W-phase plays an important role in impeding the grain growth and contributes to the alloy strengthening via dispersion strengthening mechanism [21, 30]. Moreover, some fine precipitates are homogeneously distributed at matrix in the Mg–3Zn–0.5Er alloy, as shown in Fig. 4c, d. The fine precipitate is the I-phase with its fivefold symmetry, as shown in Fig. 4d and Table 2. The presence of the nanoscale I-phase modifies the texture via DRX [30]. As a result, it will play an important role in advancing mechanical properties significantly via precipitation strengthening mechanism [12, 18].

3.3 Mechanical properties and anisotropy

Figure 5 shows stress–strain curves of Mg–0.5Zn, Mg–0.5Zn–0.5Er and Mg–3Zn–0.5Er alloys at ambient temperature. The corresponding mechanical properties such as yield strength (YS), ultimate tensile strength (UTS) and elongation (ε) in tensile directions of RD, 45° and TD are

summarized in Table 3. The values of UTS and YS along RD and 45° tensile direction display an increase tendency as the Zn content increases, respectively. The Mg–3Zn–0.5Er alloy displays the highest tensile strength along the tensile direction of RD and 45°, respectively. Along the tensile direction of RD, the values of UTS, YS and ε are 231 MPa, 191 MPa and 3.8%, respectively. Furthermore, along the tensile direction of 45°, the values of UTS, YS and ε are 250 MPa, 189 MPa and 7.3%, respectively. Meanwhile, the Mg–0.5Zn alloy shows the highest tensile strength along the tensile direction of TD, and the values of UTS, YS and ε are 213 MPa, 179 MPa and 4.6%, respectively. It suggests that the Er-containing magnesium alloy exhibits mostly higher strength, especially for the Mg–3Zn–0.5Er alloy in RD and 45° tensile direction, which is mostly ascribed to the solution hardening, nanoscale precipitation and grain refinement. Moreover, the Mg–0.5Zn–0.5Er alloy exhibits smaller in-plane anisotropy in YS, and it is related to the special “split” texture with low intensity due to shear bands and W-phase.

The strain hardening exponent (n -value) and plastic strain ratio (Lankford value, r -value) are two key parameters for the formability of materials. Thus, additional tensile tests were conducted at room temperature. The n -value and r -value are listed in Tables 3 and 4, respectively. The n -value controls a resistance of metal for plastic instability [31]. In addition, the average n -value ($\bar{n} = (n_{RD} + 2n_{45} + n_{TD})/4$) is related to the stretch formability. The r -values ($r = \varepsilon_w/\varepsilon_t$) of sheets were calculated, where ε_w and ε_t are the width-direction and the thickness-direction strains at uniaxial tension, respectively. The average r -value ($\bar{r} = (r_{RD} + 2r_{45} + r_{TD})/4$) and the planar anisotropy value ($\Delta r = (r_{RD} - 2r_{45} + r_{TD})/2$) are the key characteristics for the sheet metal forming

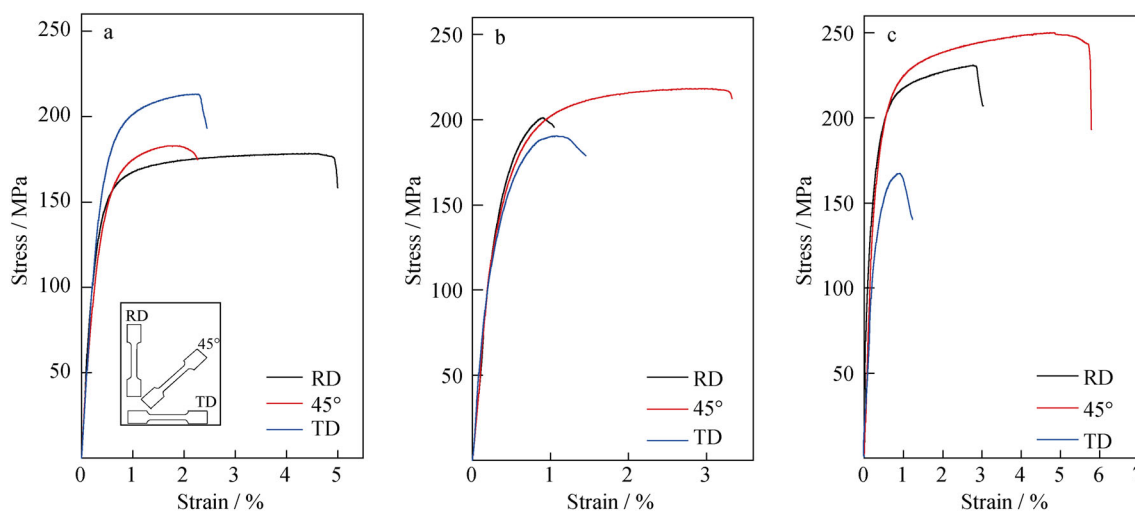


Fig. 5 Stress–strain curves of as-rolled alloys with different tensile directions (RD, 45° and TD) at room temperature: **a** Mg–0.5Zn alloy, **b** Mg–0.5Zn–0.5Er alloy, and **c** Mg–3Zn–0.5Er alloy

Table 3 Tensile mechanical properties at room temperature of as-rolled magnesium alloys (YS, 0.2% yield stress; UTS, ultimate tensile stress; ϵ , elongation; n , n -value and r , r -value)

Alloys	Direction	YS/MPa	UTS/MPa	$\epsilon/\%$	n	r
Mg-0.5Zn	RD	147 ± 2.5	178 ± 4.2	10.6 ± 4.5	0.10	0.59
	45°	157 ± 3.3	183 ± 3.9	4.2 ± 4.7	0.16	0.81
	TD	179 ± 2.8	213 ± 3.5	4.6 ± 3.5	0.13	0.59
Mg-0.5Zn-0.5Er	RD	180 ± 1.9	201 ± 5.2	2.7 ± 3.4	0.24	0.46
	45°	173 ± 2.5	218 ± 4.8	3.7 ± 2.9	0.14	0.48
	TD	165 ± 3.6	190 ± 3.9	3.4 ± 3.2	0.20	0.34
Mg-3Zn-0.5Er	RD	191 ± 3.2	231 ± 2.3	3.8 ± 4.3	0.10	0.36
	45°	189 ± 4.3	250 ± 3.5	7.3 ± 3.8	0.12	0.51
	TD	150 ± 2.9	167 ± 2.8	3.6 ± 3.5	0.16	0.31

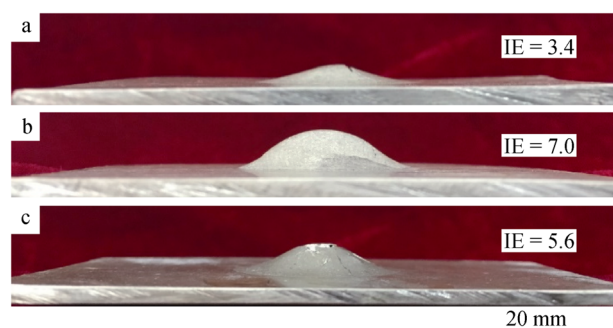
Table 4 Parameters of stretch formability of as-rolled magnesium alloys (\bar{n} , average n -value; \bar{r} , average r -value; Δr , planar anisotropy)

Alloys	\bar{n}	\bar{r}	Δr
Mg-0.5Zn	0.14	0.70	- 0.22
Mg-0.5Zn-0.5Er	0.18	0.44	- 0.08
Mg-3Zn-0.5Er	0.13	0.42	- 0.27

[2, 6, 32]. In general, the sheet with a low \bar{r} would lead to a high limiting drawing ratio (LDR). The Δr indicates a strain distribution in the sheet plane and shows a tendency for early behavior at deep draw cups. In the present work, the values of \bar{n} for Mg-0.5Zn, Mg-0.5Zn-0.5Er and Mg-3Zn-0.5Er alloys are 0.14, 0.18 and 0.13, respectively. Moreover, the values of the corresponding \bar{r} are 0.70, 0.44 and 0.42, respectively. The value of \bar{n} in the Mg-0.5Zn-0.5Er alloy is higher than that of other alloys. The Mg-0.5Zn-0.5Er and Mg-3Zn-0.5Er alloys have the similar \bar{r} value, which is much lower than that of Mg-0.5Zn alloy. It is well known that the large n -value is related to the reduction in plastic instability, which will result in enhancement of stretching capability [31]. The low \bar{r} -value suggests that the sheet thinning can easily occur during the in-plane tensile deformation, resulting in the decrease in the mechanical anisotropy and providing a comparable hardening curve (Fig. 5b) [6, 33]. It should be noted that the low \bar{r} is mainly ascribed to the addition of RE elements [2]. The sheets with low Δr value exhibit less earing tendency commonly. Therefore, the Mg-0.5Zn-0.5Er alloy sheet would appear less earing possibility during the stamping forming on account of its relatively low Δr value, which seems to have a deep connection with a low YS anisotropy.

3.4 Stretch formability at ambient temperature

Figure 6 shows the results of the Erichsen tests at room temperature. Mg-0.5Zn-0.5Er and Mg-3Zn-0.5Er alloy

**Fig. 6** Macro-photographs of specimens after Erichsen test at room temperature: **a** as-rolled Mg-0.5Zn alloy, **b** as-rolled Mg-0.5Zn-0.5Er alloy, and **c** as-rolled Mg-3Zn-0.5Er alloy

sheets exhibit more excellent stretch formability with Erichsen values (IE) of 7.0 and 5.6 mm, respectively, which are better than that of Mg-0.5Zn alloy (IE = 3.4 mm). In particular, the IE value of Mg-0.5Zn-0.5Er alloy is twice as high as that of Mg-0.5Zn alloy. As stated above, the stretch formability of materials has a closed relationship with some parameters such as n -value and r -value. Large n -value plays an important role in enhancing stretch formability [22]. Low r -value indicates that the thickness-direction strain is almost the same as that of the width-direction strain, which contributes to the uniform forming [2]. Therefore, typically high n -value and low r -value can be beneficial to stretch formability [6, 22, 33]. In this investigation, the Mg-0.5Zn-0.5Er alloy with larger n -value and lower r -value shows an outstanding IE value, which is consistent with that reported by Chino et al. [2]. Moreover, the values of n and r affect the stretch formability by regulating basal texture intensity and splitting of the basal plane. Meanwhile, the Mg-0.5Zn alloy that contains Er free sheet exhibits a larger \bar{r} value and a similar \bar{n} value because of the great increase in the texture intensity compared with Mg-0.5Zn-0.5Er alloy. Meanwhile, Mg-0.5Zn-0.5Er alloy displays a larger \bar{n} and a similar \bar{r} . It is evidenced by the RD-split texture contrasting with the Mg-3Zn-0.5Er alloy. Thus, it is concluded that the stretch

formability of magnesium sheets is determined by intensity and distribution of basal texture.

4 Conclusion

The effect of trace addition of Zn/Er on microstructure, texture and formability of Mg–Zn–Er alloys was investigated. The main conclusions are shown below.

The trace addition of Er (e.g., 0.5 wt%) into the Mg–Zn alloys weakened the basal texture significantly via activation of the non-basal slip. The RD-split texture was directly attributed to shear bands, which were caused by DRX of the $\{10\bar{1}1\}$ compression and $\{10\bar{1}1\}$ – $\{10\bar{1}2\}$ double twins. The regulation of Zn/Er ratio determined the type of second phases, consequently the nanoscale W-phase precipitated only in the Mg–0.5Zn–0.5Er alloy (Zn/Er = 1.0), and I-phase only in the Mg–3Zn–0.5Er alloy (Zn/Er = 6.0). The W-phase distributed at both grain boundaries and subgrains, and it strengthened the alloys via dispersion strengthening mechanism, whereas the nanoscale I-phase mainly precipitated in the grain interiors and hence it can strengthen the alloy via precipitation strengthening mechanism. The Mg–0.5Zn–0.5Er alloy exhibits excellent stretch formability with Erichsen value of 7.0 mm, which is higher than those of Mg–3Zn–0.5Er (5.6 mm) and Mg–0.5Zn (3.4 mm) alloys, respectively. The higher Erichsen value for the Mg–0.5Zn–0.5Er alloy derived from weak and random basal texture, which resulted in high n -value, small r -value and low anisotropy (Δr). In addition, this alloy exhibited good tensile properties along RD with a YS of (180.0 ± 1.9) MPa, UTS of (201.0 ± 5.2) MPa and elongation to failure of $(2.7 \pm 3.4)\%$. The good performance was attributed to the formation of shear bands and precipitation of nanoscale W-phase ($\text{Mg}_3\text{Zn}_3\text{Er}_2$).

Acknowledgements The work was financially supported by Beijing Natural Science Foundation (No. 2172013), the National Key Research and Development Program (No. 2016YFB0301101), Beijing Municipal Commission of Education Key Science, Technology Projects (No. KZ201810005005) and the National Natural Science Foundation of China (No. 51801048).

References

- [1] Zhang YJ, Yan CW, Wang FH, Li WF. Electrochemical behavior of anodized Mg alloy AZ91D in chloride containing aqueous solution. *Corros Sci.* 2005;47(11):2816.
- [2] Chino Y, Kado M, Mabuchi M. Enhancement of tensile ductility and stretch formability of magnesium by addition of 0.2 wt% (0.035 at%) Ce. *Mater Sci Eng, A.* 2008;494(1-2):343.
- [3] Trang TTT, Zhang JH, Kim JH, Zargaran A, Hwang JH, Suh BC, Kim NJ. Designing a magnesium alloy with high strength and high formability. *Nat Commun.* 2018;9(1):2522.
- [4] Zhang JH, Liu SJ, Wu RZ, Hou LG, Zhang ML. Recent developments in high-strength Mg-RE-based alloys: focusing on Mg-Gd and Mg-Y systems. *J Magn Alloys.* 2018;6(3):277.
- [5] Suh J, Hernández JV, Letzig D, Golle R, Volk W. Enhanced mechanical behavior and reduced mechanical anisotropy of AZ31 Mg alloy sheet processed by ECAP. *Mater Sci Eng, A.* 2016;650(5):523.
- [6] Suh J, Hernández JV, Letzig D, Golle R, Volk W. Effect of processing route on texture and cold formability of AZ31 Mg alloy sheets processed by ECAP. *Mater Sci Eng, A.* 2016; 669(4):159.
- [7] Kaseem M, Chung BK, Yang HW, Hamad K, Ko YG. Effect of deformation temperature on microstructure and mechanical properties of AZ31 Mg alloy processed by differential-speed rolling. *J Mater Sci Technol.* 2015;31(05):498.
- [8] Luo D, Wang HY, Zhao LG, Wang C, Liu GJ, Liu Y, Jiang QC. Effect of differential speed rolling on the room and elevated temperature tensile properties of rolled AZ31 Mg alloy sheets. *Mater Charact.* 2017;124:223.
- [9] Yan H, Xu SW, Chen RS, Kamado S, Honma T, Han EH. Twins, shear bands and recrystallization of a Mg-2.0%Zn-0.8% Gd alloy during rolling. *Scr Mater.* 2011;64(2):141.
- [10] Stanford N. Micro-alloying Mg with Y, Ce, Gd and La for texture modification-A comparative study. *Mater Sci Eng A.* 2010;527(10–11):2669.
- [11] Basu I, Al-Samman T. Twin recrystallization mechanisms in magnesium-rare earth alloys. *Acta Mater.* 2015;96:111.
- [12] Tian Y, Huang H, Yuan GY, Chen CL, Wang ZC, Ding WJ. Nanoscale icosahedral quasicrystal phase precipitation mechanism during annealing for Mg-Zn-Gd-based alloys. *Mater Lett.* 2014;130:236.
- [13] Liu P, Jiang HT, Cai ZX, Kang Q, Zhang Y. The effect of Y, Ce and Gd on texture, recrystallization and mechanical property of Mg-Zn alloys. *J Magn Alloys.* 2016;4(3):188.
- [14] Al-Samman T, Li X. Sheet texture modification in magnesium-based alloys by selective rare earth alloying. *Mater Sci Eng, A.* 2011;528(10–11):3809.
- [15] Yan H, Chen RS, Zheng N, Luo J, Kamado S, Han EH. Effects of trace Gd concentration on texture and mechanical properties of hot-rolled Mg-2Zn-xGd sheets. *J Magn Alloys.* 2013;1(1):23.
- [16] Liu BS, Li HX, Ren YP, Jiang M, Qin GW. Phase equilibria of low-Y side in Mg-Zn-Y system at 400 °C. *Rare Met.* 2020; 39(3):262.
- [17] Liu K, Wang QF, Du WB, Li SB, Wang ZH. Failure mechanism of as-cast Mg-6Zn-2Er alloy during tensile test at room temperature. *Trans Nonferrous Met Soc China.* 2013;23(11):3193.
- [18] Liu K, Sun CC, Wang ZH, Li SB, Wang QF, Du WB. Microstructure, texture and mechanical properties of Mg-Zn-Er alloys containing I-phase and W-phase simultaneously. *J Alloys Compd.* 2016;665:76.
- [19] Wang QF, Liu K, Wang ZH, Li SB, Du WB. Microstructure, texture and mechanical properties of as-extruded Mg-Zn-Er alloys containing W-phase. *J Alloys Compd.* 2014;602:32.
- [20] Wu HR, Du WB, Li SB, Liu K, Wang ZH. Microstructure and mechanical properties of AZ31 magnesium alloy reinforced by I-phase. *Rare Met.* 2019;38(8):733.
- [21] Zeng ZR, Zhu YM, Xu SW, Bian MZ, Davies CHJ, Birbilis N, Nie JF. Texture evolution during static recrystallization of cold-rolled magnesium alloys. *Acta Mater.* 2016;105:479.
- [22] Chino Y, Huang XS, Suzuki K, Sassa K, Mabuchi M. Influence of Zn concentration on stretch formability at room temperature of Mg-Zn-Ce alloy. *Mater Sci Eng A.* 2010;528(2):566.
- [23] Barnett MR, Nave MD, Bettles CJ. Deformation microstructures and textures of some cold rolled Mg alloys. *Mater Sci Eng A.* 2004;386(1):205.

- [24] Basu I, Al-Samman T, Gottstein G. Shear band-related recrystallization and grain growth in two rolled magnesium-rare earth alloys. *Mater Sci Eng A*. 2013;579(9):50.
- [25] Guo F, Zhang DF, Yang XS, Jiang LY, Chai SS, Pan FS. Effect of rolling speed on microstructure and mechanical properties of AZ31 Mg alloys rolled with a wide thickness reduction range. *Mater Sci Eng A*. 2014;619:66.
- [26] Xu SW, Kamado S, Matsumoto N, Honma T, Kojima Y. Recrystallization mechanism of as-cast AZ91 magnesium alloy during hot compressive deformation. *Mater Sci Eng A*. 2009; 527(1):52.
- [27] Drouven C, Basu I, Al-Samman T, Korte-Kerzel S. Twinning effects in deformed and annealed magnesium-neodymium alloys. *Mater Sci Eng A*. 2015;647:91.
- [28] Kim KH, Suh BC, Bae JH, Shim MS, Kim S, Kim NJ. Microstructure and texture evolution of Mg alloys during twin-roll casting and subsequent hot rolling. *Scr Mater*. 2010; 63(7):716.
- [29] Su J, Sanjari M, Syed A, Kabir H, Jung IH, Yue S. Dynamic recrystallization mechanisms during high speed rolling of Mg-3Al-1Zn alloy sheets. *Scr Mater*. 2016;113:198.
- [30] Hantzsche K, Bohlen J, Wendt J, Kainer KU, Yi SB, Letzig D. Effect of rare earth additions on microstructure and texture development of magnesium alloy sheets. *Scr Mater*. 2010;63(7): 725.
- [31] Agnew SR, Duygulu Ö. Plastic anisotropy and the role of non-basal slip in magnesium alloy AZ31B. *Int J Plast*. 2005; 21(6):1161.
- [32] Li X, Al-Samman T, Gottstein G. Mechanical properties and anisotropy of ME20 magnesium sheet produced by unidirectional and cross rolling. *Mater Des*. 2011;32(8):4385.
- [33] Wu D, Chen RS, Han EH. Excellent room-temperature ductility and formability of rolled Mg-Gd-Zn alloy sheets. *J Alloys Compd*. 2011;509(6):2856.